

**Hidden dependence of spreading vulnerability on topological complexity**

Mark M. Dekker\*

*Department of Information and Computing Sciences, Utrecht University, Princetonplein 5, 3584 CC Utrecht, The Netherlands*

Raoul D. Schram

*Information and Technology Services, Heidelberglaan 8, 3584 CS Utrecht, The Netherlands*

Jiamin Ou

*Department of Sociology, Utrecht University, Padualaan 14, 3584 CH Utrecht, Netherlands*Debabrata Panja *Department of Information and Computing Sciences, Utrecht University, Princetonplein 5, 3584 CC Utrecht, The Netherlands*

(Received 3 December 2021; accepted 8 April 2022; published 5 May 2022)

Many dynamical phenomena in complex systems concern spreading that plays out on top of networks with changing architecture over time—commonly known as temporal networks. A complex system’s proneness to facilitate spreading phenomena, which we abbreviate as its “spreading vulnerability,” is often surmised to be related to the topology of the temporal network featured by the system. Yet, cleanly extracting spreading vulnerability of a complex system directly from the topological information of the temporal network remains a challenge. Here, using data from a diverse set of real-world complex systems, we develop the “entropy of temporal entanglement” as a quantity to measure topological complexities of temporal networks. We show that this parameter-free quantity naturally allows for topological comparisons across vastly different complex systems. Importantly, by simulating three different types of stochastic dynamical processes playing out on top of temporal networks, we demonstrate that the entropy of temporal entanglement serves as a quantitative embodiment of the systems’ spreading vulnerability, irrespective of the details of the processes. In being able to do so, i.e., in being able to quantitatively extract a complex system’s proneness to facilitate spreading phenomena from topology, this entropic measure opens itself for applications in a wide variety of natural, social, biological, and engineered systems.

DOI: [10.1103/PhysRevE.105.054301](https://doi.org/10.1103/PhysRevE.105.054301)**I. INTRODUCTION**

Networks, consisting of system elements (agents) and their interactions by nodes and links respectively, have proved to be effective tools for analyzing complex systems. For a large variety of them, notable emergent dynamical phenomena of interest concern spreading, effected by individual agents playing the role of carriers and transmitting to others as they interact, e.g., sharing information through conversations [1,2], passing of signals among animals [3,4] and of infectious disease pathogens [5,6], purveyance of (fake) news [7], synchronicity in neuronal spikes [8,9], and cascading dynamics in sociotechnical systems [10–13]. When the agents’ identities and the precise sequences and timings of their interactions over a given time interval are compiled together into a temporal network [13–18], it becomes evident that spreading is actually a dynamical process taking place on top of the network.

From this, it seems natural to expect that the topological complexity of a temporal network will have a profound

influence on the system’s proneness to facilitate spreading phenomena—we abbreviate the latter as its spreading vulnerability (quantified later in the paper)—e.g., the formation and dispersion of epidemiological bubbles or echo chambers will dictate *how quickly, or efficiently*, pathogens or (fake) news may spread. However, establishing a quantitative relation between the two, from which the system’s spreading vulnerability can be extracted directly from the topological complexity of the temporal network featured by the system, remains a challenge. The key obstacle stems from the heterogeneities in the agent interactions intrinsic to temporal networks in the temporal domain—there simply are no rules to guide which agent may interact with which others, when, for how long, and in which precise sequence—that need to be suitably combined with the topological complexities that are already present in the network of agent-to-agent contacts at any given time. Note that the latter, i.e., the agents’ contact network at any given time, is in fact a *static* network, for which methods to deal with heterogeneities are already well established in the forms of degree distribution, various forms of centrality measures, and community detection algorithms [19].

Here we develop an insightful quantity to measure topological complexities of temporal networks: We name it the *entropy of temporal entanglement* (the choice for this name

\*Present address: Centre for Complex Systems Studies, Utrecht University, Minnaertgebouw, Leuvenlaan 4, 3584 CE Utrecht, The Netherlands.

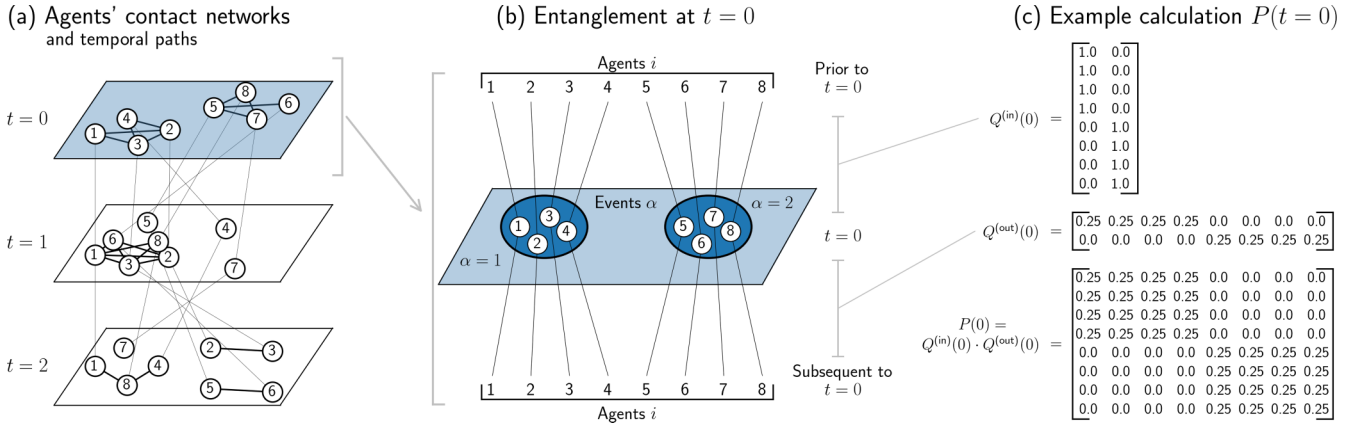


FIG. 1. Temporal entanglement. (a) An example of a temporal network, in terms of agent-to-agent contacts as interactions among eight numbered agents, at snapshots taken at integer units of sampling time. Snapshots are shown as time layers; the agent-to-agent contacts at integer times are shown as black links within the corresponding time layer. The agents' temporal paths (strings) from one snapshot to the next are shown as gray lines. The changes in the topology of the agent-to-agent contacts from one snapshot to the next make the strings weave through and entangle with each other. (b) Entanglement of the strings at  $t = 0$ , extracted from panel (a); shown explicitly are the temporal paths (strings), labeled by Roman agent indices, and the events in dark blue circles, labeled by Greek indices. Events are the connected components of the agents' contact network at  $t = 0$ . (c) Calculation of the agent-to-agent propagator matrix  $P(0)$  as  $P(0) = Q^{(in)}(0)Q^{(out)}(0)$ . The  $i\alpha$ th element of the agent-to-event propagator matrix  $Q^{(in)}(0)$  is the probability of a random walker to start at agent  $i$  prior to  $t = 0$  and end at event  $\alpha$  at  $t = 0$  in one hop. Similarly, the  $\alpha i$ th element of the event-to-agent propagator matrix  $Q^{(out)}(0)$  is the probability of a random walker to start at event  $\alpha$  at  $t = 0$  and end at agent  $i$  subsequent to  $t = 0$  in one hop.

is justified below, and it bears no connection to entanglement entropy for quantum many-body systems). Using real-world temporal networks data, and simulating three different dynamical processes on top of them, we show that this entropic measure not only allows for a quantitative comparison of vastly different complex systems, but crucially it also bears a clean relation to the system's spreading vulnerability, irrespective of the details of the processes. In other words, this entropic measure is able to directly and cleanly extract a complex system's proneness to facilitate spreading phenomena from its topology.

We use the term “entanglement” because of the following. Real-world temporal networks often follow a discrete time convention, wherein the agents' interactions, denoted by agent-to-agent contacts, are sampled at some fixed interval (which we denote as  $\tau_s$ ): An example is shown in Fig. 1(a), where the temporal network consists of layers in time, denoted in integer units of  $\tau_s$ . Then the gray lines denoting the agents' temporal paths across the layers in Fig. 1(a)—obtained by following individual agents in time—resemble strings laid out in time. Changes in agent interactions, i.e., in agent-to-agent contacts, from one snapshot to the next make the strings weave through and *entangle* with each other. (In the absence of any interactions among the agents at integer times, the strings will simply be parallel to each other, without any entanglement.)

## II. SUMMARY CALCULATION OF THE ENTROPY OF TEMPORAL ENTANGLEMENT

We begin by introducing “events.” Events are the connected components of the agents' contact networks at integer times. An example can be found in Figs. 1(a) and 1(b), where the interactions among agents 1 through 4 and agents 5 through 8 constitute two distinct events at  $t = 0$ . In this

definition, every agent becomes a part of a single event, and all agents are equivalent within an event; in addition, some may be solo-agent events, as seen at  $t = 1$  in Fig. 1(a). [Note also that the equivalence of agents within an event does not respect the precise agent-to-agent contacts within events, such as the absence of a direct contact between agents 1 and 4 at  $t = 0$  in Fig. 1(a), while all the others are in direct contact in that event; we take this up in the paragraph below Eq. (3).]

We then probe the topology of a temporal network, consisting of  $N$  agents, using random walkers hopping along the agents' temporal paths forward in time. (Probing network topology using random walkers is a common practice.) The entire procedure is parameter-free, and is formally described in Appendix A 1. We summarize it here for  $m$  events at time  $t$  in three steps; a rendering of them for the example system in Fig. 1(a) with  $N = 8$  and  $m = 2$  at  $t = 0$ , and the corresponding calculations are shown in Figs. 1(b) and 1(c). (1) Using Roman and Greek letter indices to denote agents and events respectively, we construct the  $N \times m$  agent-to-event propagator matrix  $Q^{(in)}(t)$ , with matrix element  $Q_{i\alpha}^{(in)}$  denoting the probability for a random walker to start at agent  $i$  prior to  $t$  and reach event  $\alpha$  at (integer) time  $t$  in one hop. (2) Similarly, we construct the  $m \times N$  event-to-agent propagator matrix  $Q^{(out)}(t)$ , with matrix element  $Q_{\alpha i}^{(out)}$  denoting the probability for a random walker, to start at event  $\alpha$  at time  $t$  and reach agent  $i$  subsequent to time  $t$  in one hop. (For both steps, the hops are thus coupled to the sampling time interval  $\tau_s$ .) (3) Finally, we construct the  $N \times N$  agent-to-agent propagator matrix as

$$P(t) = Q^{(in)}(t)Q^{(out)}(t). \quad (1)$$

Upon extending this procedure to finite (integer) interval  $\Delta t$  leads us to the product matrix  $\wp(t, \Delta t) = P(t)P(t + 1)P(t + 2) \dots P(t + \Delta t)$  that similarly contains the full

entanglement information in the finite time interval  $[t, t + \Delta t]$ . By construction, the matrix element  $\wp_{ij}(t, \Delta t)$  is the probability of a random walker starting at agent  $i$  prior to time  $t$  to end up at agent  $j$  subsequent to time  $(t + \Delta t)$  following the agents' temporal paths. This allows us to define

$$s_i(t, \Delta t) = - \sum_j \wp_{ij}(t, \Delta t) \ln \wp_{ij}(t, \Delta t) \quad (2)$$

as the (information-theoretic) entropy associated with the random walker starting at agent  $i$  prior to time  $t$ . A further sum over  $i$ , weighing each starting random walker equally, provides a network-wide (global) sum of the  $s_i(t, \Delta t)$  entropies, allowing us to define the entropy of temporal entanglement for all agents over the interval  $[t, t + \Delta t]$  as

$$S(t, \Delta t) = - \frac{1}{N \ln N} \sum_{i,j} \wp_{ij}(t, \Delta t) \ln \wp_{ij}(t, \Delta t). \quad (3)$$

Given that  $s_j(t, \Delta t)$  is upper bounded by  $\ln N$  and the equal weight given to each of the  $N$  random walkers for calculating the entropy of temporal entanglement,  $N \ln N$  factor in the denominator of  $S(t, \Delta t)$  ensures  $S(t, \Delta t) \in [0, 1]$ .

Construction of the entropy of temporal entanglement that respects the precise agent-to-agent contacts within events [such as the absence of a direct contact between agents 1 and 4 at  $t = 0$  in Fig. 1(a), while all the others are in direct contact in that event] follows a line similar to the above, albeit it is slightly more involved. The corresponding entropy of temporal entanglement  $S_c$ , formally derived in Appendix A, is also parameter-free and fully determined by the topology of the network. In Appendix A, we argue that with decreasing sampling time interval  $\tau_s$ ,  $S_c$  approaches  $S$ , the entropy of temporal entanglement as calculated in Eqs. (1)–(3) in terms of the connected components of the agents' contact networks, which we henceforth adhere to.

### III. PROPERTIES AND INTERPRETATION OF THE ENTROPY OF TEMPORAL ENTANGLEMENT

Three insightful attributes of  $S(t, \Delta t)$  are critical for being able to extract a complex system's proneness to facilitate spreading phenomena. These are the following: (1)  $S(t, \Delta t)$  represents the agents' mixing (i.e., mingling) propensity in the interval  $[t, t + \Delta t]$  (we explore this further in Sec. III B below), (2) it respects the *temporal sequence* of agent interactions, and (3) in building up the sequences forward in time, it automatically incorporates *causality*: note that a spreading phenomenon in the past can influence its future dynamics, but not *vice versa*. While (2) and (3) can be gleaned from how  $\wp$  is built from the  $P$  matrices, (1) follows from that  $\wp_{ij}(t, \Delta t)$  is the probability of a random walker starting at agent  $i$  prior to time  $t$  to end up at agent  $j$  subsequent to time  $(t + \Delta t)$  following temporal paths: the more distinct temporal paths there are to trace a given agent  $i$  back from any agent  $j$ , the more nonzero  $\wp_{ij}$  elements there are. These attributes further translate to the following useful properties of  $S(t, \Delta t)$ . (a) An agent, who never interacts with another in the interval  $[t, t + \Delta t]$ , has zero contribution to  $S(t, \Delta t)$ . This, in fact, is the basis for why small  $S(t, \Delta t)$  corresponds to a highly fragmented temporal network, i.e., large number of disjoint

components in the interval  $[t, t + \Delta t]$ , possibly with many agents separated from each other throughout the interval. (b) It allows us to quantify the contribution of an individual agent to entanglement, which we take up in Appendix B. (c) Typically, an increasing  $\Delta t$  would imply more nonzero  $\wp_{ij}$ 's: More distinct temporal paths become available to trace a given agent  $i$  back from any agent  $j$ . This implies that for any value of  $t$ ,  $S(t, \Delta t)$  is monotonic in  $\Delta t$ , e.g., as can be seen in Figs. 2(a) and 2(b); for a fixed value of  $\Delta t$ , however,  $S(t, \Delta t)$  is nonmonotonic in  $t$ .

In contrast to the above, the practice of aggregating the agents' contact networks over a certain time interval for a temporal network into a static one [2,13,15,16,20] discards the precise sequences and durations of agent interactions. As for methods that do capture heterogeneities in the temporal domain by means of, e.g., checking how communities evolve in time [21,22], constructing temporal counterparts of degree and betweenness [23], or treating a temporal network as a multilayer one with layers representing discrete time snapshots [24], we note the following. The emphasis of temporal betweenness on shortest paths makes it ideal to identify topological centrality, but for the application of spreading vulnerability, path *lengths* are only important in terms of which agents are traceable in a fixed time interval. Of critical importance for spreading vulnerability are the exact interaction sequences and frequencies, which are considerably less focused on in the existing literature. Likewise, concerning community detection approaches, under time reversal, the community structure in the multilayer network will remain invariant, while the dynamics of a process taking place on top of the temporal network will be profoundly different.

#### A. Entropy of temporal entanglement represents the agents' mixing propensity

In order to demonstrate that the entropy of temporal entanglement has a clear relationship to the agents' propensity to mixing, we consider two temporal network data sets that track student contacts respectively in a high school and a primary school by wearable sensors, sampled at 20-s intervals [2,25,26] (details on the data in Appendix B). Per data set, in Figs. 2(a) and 2(b) we plot the time evolution of  $S(t, \Delta t)$  for four different  $\Delta t$  values, varying  $t$  over one full school day. Further, delving into the (publicly available) metadata, in Figs. 2(c) and 2(d) we plot the contact networks of the agents aggregated over two 5-min intervals, one each for high and low values of  $S(t, \Delta t)$ . The correspondence between the top and the bottom panels demonstrates that the students' mixing behavior, adapting to changing school circumstances, is being reflected in the topological complexity of the temporal network, which in turn is being captured by the entropy of temporal entanglement (school breaks invite more mixing in comparison to being separated in classrooms, and correspondingly lead to more topological complexity and higher entropy of temporal entanglement).

Given the above, an unbiased (e.g., from number of agents, sampling time interval) cross-system comparison of topological complexities of temporal networks requires two rescaling operations. The first (natural) one is that  $\Delta t$  must be replaced by  $\Delta e$ , the average number of events per agent in the interval

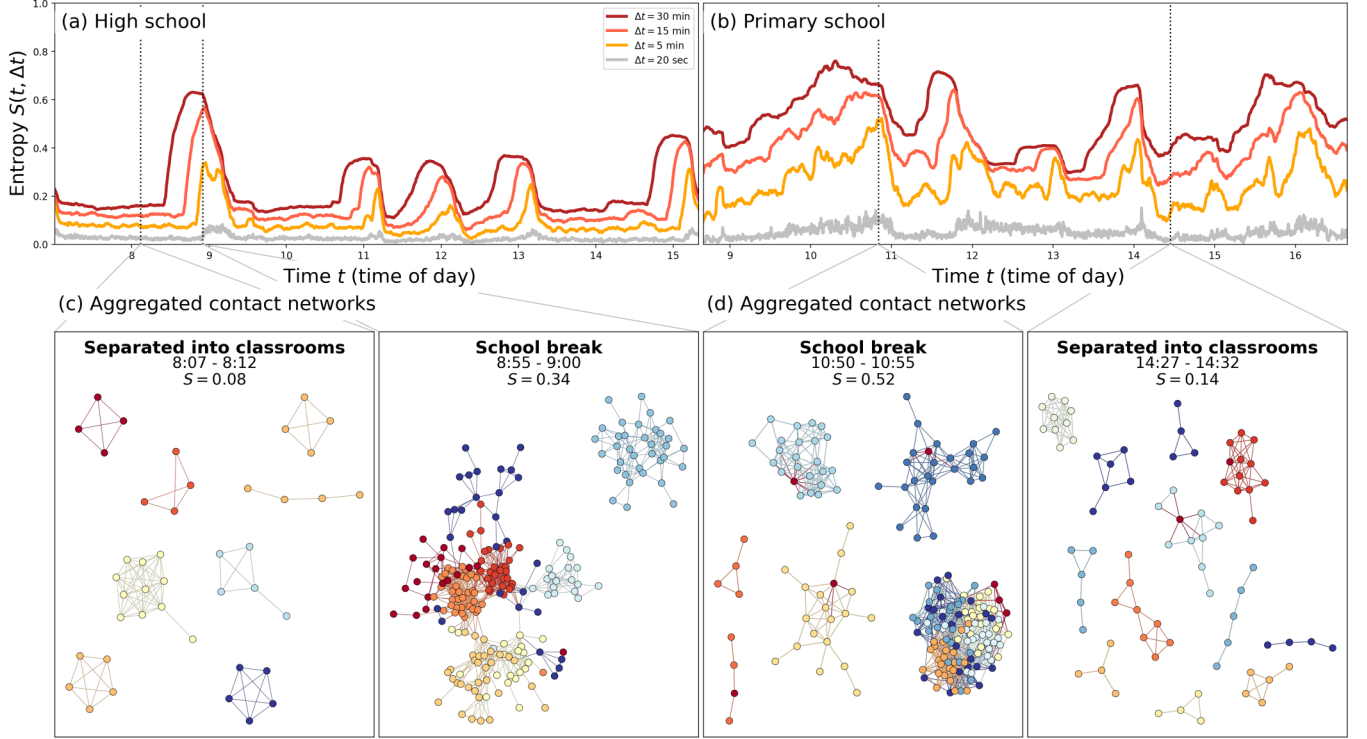


FIG. 2. Entropy of temporal entanglement for two real-world temporal networks: contacts among high school (Thiers13 data set day 2, left column) and primary school (LyonSchool data set day 1, right column) students. [(a), (b)]  $S(t, \Delta t)$  for four values of  $\Delta t$ : 20 s (gray), 5 min (orange), 15 min (red), and 30 min (darker red); for any value of  $t$ , note that  $S(t, \Delta t)$  is monotonically increasing with  $\Delta t$ ; and  $x$  axes denote the time of day. Vertical dashed lines correspond to 5-min intervals, expanded in panels (c) and (d), chosen to reflect one high-entropy and one low-entropy situation per panel. [(c), (d)] Aggregated contact networks within the 5-min intervals (only connected components with at least 4 students are shown), demonstrating high (resp. low) connectivity in high- $S$  (resp. low- $S$ ) cases. Metadata reveal that the situations correspond to school breaks and ongoing classes respectively (students belonging to the same classroom are represented by the same node color).

$\Delta t$  (the assumption here is that the agents' contact networks are sampled frequently enough such that contact sequences are fully captured). The second one concerns normalizing the entropy to define a standardized mixing propensity:

$$s(\Delta e) = \frac{1}{T} \sum_{t=0}^T \frac{S(t, \Delta e)}{S(t, \Delta e_0)}, \quad (4)$$

where  $\Delta e_0$  is a constant for standardization. Note that  $s(\Delta e)$  is a monotonically increasing function of  $\Delta e$  since  $S(t, \Delta t)$  is a monotonically increasing function of  $\Delta t$ . Plotting  $s(\Delta e)$  vs  $\Delta e$  in a log-log plot in Fig. 3(a), using  $\Delta e_0 = 5$ , we observe the differences in how characteristically quickly  $s(\Delta e)$  builds up in different real-world systems (see Appendix B for details on the systems). (Even though  $\Delta e_0$  is merely a standardization parameter, it should be chosen large enough to have some stability in the plot. We have experimented with other values such as  $\Delta e_0 = 1$  and the results do not substantially differ.) We analyze this further in Appendix A to demonstrate that the fastest rate of increase in the entropy of temporal entanglement is achieved when the agents' contact sequences, in the temporal domain, only contain trees. Real-world temporal networks of course contain loops (e.g., due to repetitive interactions among agents); note also that social contacts are often structured in bubbles, which enhances the chances of having loops.

## B. Entropy of temporal entanglement is an embodiment of systems' vulnerability to spreading phenomena

We begin by quantifying spreading vulnerability of a complex system, which requires adding dynamical processes on top of the temporal network that the system features. For this purpose, we consider three different types of stochastic processes: (1) a majority-vote model that simulates the opinion on a dilemma that spreads through events by means of the majority votes, (2) a transport delay model, where delay spreads through events due to all the participants copying the delay of the maximally delayed agent, and (3) an epidemiological susceptible-infected (SI) model with infection probability  $\beta = 0.8$ . Details of the models and their backgrounds can be found in Appendix C. The corresponding process variables are respectively expressed as  $V_i(t, \Delta t)$ , with  $i \in \{\text{maj}, \text{del}, \text{dis}\}$ , and just like the entropy of temporal entanglement  $S(t, \Delta t)$ , they are normalized to the interval  $[0, 1]$  (elaborated in Appendix C). Like  $S(t, \Delta t)$ , for any given  $t$ ,  $V_i(t, \Delta t)$  is a monotonically increasing function of  $\Delta t$ , and the spreading vulnerability is quantified by how quickly  $V_i(t, \Delta t)$  increases as a function of  $\Delta t$ . [Also, like  $S(t, \Delta t)$ ,  $V_i(t, \Delta t)$  exhibits strong heterogeneous behavior as a function of  $t$ .]

We then simulate the above three stochastic processes for all the systems in Fig. 3(a). Using  $\Delta t = 15$  min, we plot the process variables together in Figs. 3(c) and 3(d) for the temporal network data set for interacting baboons [27] and

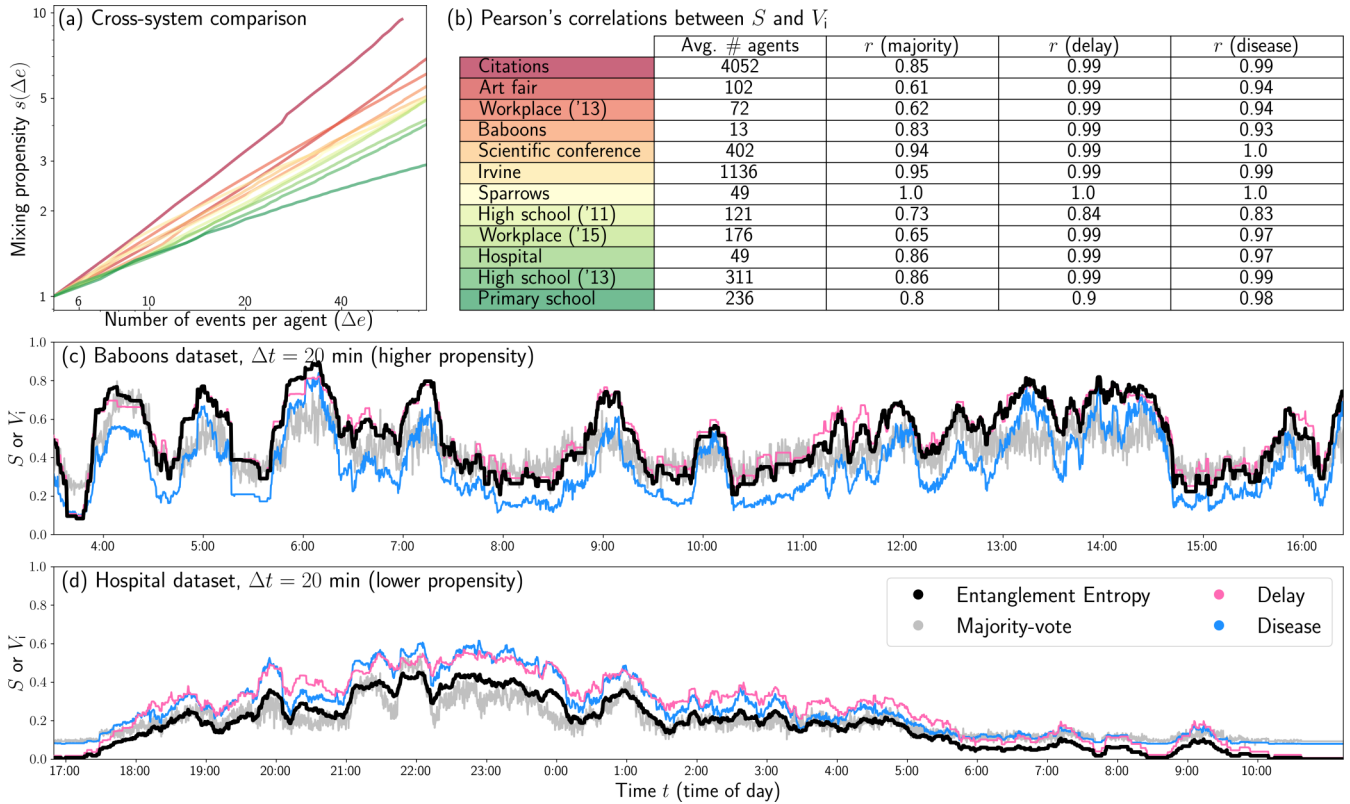


FIG. 3. Standardized mixing propensity  $s$  and the systems' vulnerability  $V$  to spreading phenomena (for precise definitions of both, see Sec. III B below). (a) Mixing propensity vs the number of events per agent as a system-characterizing property, shown for 12 complex systems: from green (slow rate of increase) to red (fast rate of increase). The systems are noted in panel (b) in the same color coding. (b) Pearson's correlation between  $S(t, \Delta t)$  and  $V_i(t, \Delta t)$ , with  $i \in \{\text{maj}, \text{del}, \text{dis}\}$ , corresponding to a majority-vote model, a transport delay model, and an epidemiological susceptible-infected (SI) model respectively (see text and Appendix B for details). (c) The full time-series of  $S(t, \Delta t)$  and  $V_i(t, \Delta t)$  on day 2 of the Baboons data set [27]. Displayed on the  $x$  axis are the times of day.  $\Delta t = 20$  min (i.e., 60 units of sampling time intervals) is used. (d) Same as in panel (c), but using day 2 of the Hospital data set [28].

hospital patients and workers [28]: Visual inspection immediately reveals that for both systems, the variations in  $S$  and  $V_i$  over time are highly synchronized. For all the complex systems in Fig. 3(a), the Pearson's correlation coefficients between  $S(t, \Delta t)$  and  $V_i(t, \Delta t)$  are tabulated in Fig. 3(b) using the same color scheme [of Fig. 3(a)]. The table clearly showcases that the entropy of temporal entanglement is essentially an embodiment of a complex system's vulnerability to spreading phenomena, irrespective of the details of the processes playing out on top of the networks. In other words, the entropy of temporal entanglement secures a clean relation between the spreading vulnerability of a complex system, and the topology of the temporal network featured by the system, and thereby, the current work indicates that computing the entropy of temporal entanglement is sufficient to quantitatively assess a complex system's proneness to facilitate spreading phenomena.

#### IV. DISCUSSION AND OUTLOOK

In summary, we have developed the entropy of temporal entanglement as a measure of topological complexity of temporal networks. By construction, it is a parameter-free quantity that embodies collective topological property at any given timescale, allowing for comparisons across

vastly different complex systems. By simulating three different dynamical processes playing out on the top of real-world temporal networks, we have demonstrated that the entropy of temporal entanglement is a good representation of the systems' spreading vulnerability, irrespective of the details of the processes—less entanglement (lower topological complexity) means lower spreading vulnerability and *vice versa*.

Let us reflect on why this topological entropy measure is such a good predictor of spreading dynamics, irrespective of the details of the dynamical processes put on top on the temporal networks. The reason can be traced back to the fact that the  $\varphi_{ij}(t, \Delta t)$  is the probability of a random walker to start at agent  $i$  prior to time  $t$ , and end up at agent  $j$  subsequent to time  $t + \Delta t$ . With  $\sum_j \varphi_{ij}(t, \Delta t) = 1$ , the time evolution of  $\varphi_{ij}(t, \Delta t)$  as a function of  $\Delta t$  can itself be seen as a spreading process starting at agent  $i$  at time  $t$ , albeit a *deterministic* one—determined entirely by the topology of the temporal network, free of any parameter. It is therefore logical that the entropy of temporal entanglement serves as a quantitative embodiment of the systems' spreading vulnerability, irrespective of the details of the processes. Nevertheless, the important fact remains that the entropy of temporal entanglement establishes a clean quantitative relation between the topological complexity of a temporal network and the system's proneness to facilitate spreading phenomena.

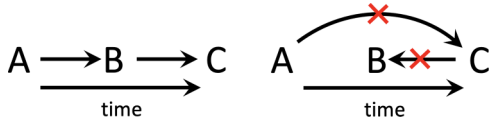


FIG. 4. Three agents A, B, and C interacting in sequence. (Left) A propagation process that is in reality allowed. (Right) A propagation process that is in reality impossible, but is allowed when the agent interactions information in the temporal dimension is collapsed.

That said, based on Figs. 3(b) and 3(d), one may potentially argue along the following lines. Instead of a sophisticated quantity like the entropy of temporal entanglement, why not simply use  $S'(t, \Delta t) = (\text{number of contacts between } t \text{ and } t + \Delta t) / [N(N - 1)/2]$  to demonstrate that the speed of spreading in the interval  $[t, t + \Delta t]$  is a direct reflection of the temporal density of agent-to-agent contacts? This is a subtle issue, and can be addressed as follows. In calculating  $S'$ , all the information on the agent interactions in the temporal dimension between  $t$  and  $t + \Delta t$  is collapsed, which erases all information on the *sequence* of agent interactions (we have mentioned this briefly in the paragraph above Sec. III A). For a spreading process, the sequence is critical: if agent A interacts with agent B, followed by B interacting with C, then the spreading process must follow the sequence  $A \rightarrow B \rightarrow C$ , while in the network obtained by collapsing the temporal dimension, since the sequential information of the agent interactions is lost, spreading can also take place from  $A \rightarrow C \rightarrow B$  (Fig. 4).

The key point this paper posits is that for a temporal network, the topological counterpart of the spreading process respecting the interaction sequence is the entropy of temporal entanglement. It is for this reason that  $S(t, \Delta t)$ , in comparison to  $S'(t, \Delta t)$ , is not simply capturing the higher order structures in a temporal network, but is actually respecting the correct sequential information of agent interactions in the topology of the network. This issue has recently been discussed more extensively in a recent paper coauthored by three of us [29].

System vulnerability is receiving progressively more attention in widely diverse areas, especially in the context of large perturbations induced by, e.g., the COVID-19 pandemic, species' habitat loss and fragmentation, disruption of food webs, and robustness of biological systems such as gene regulation, metabolism, neural dynamics, and engineered systems. The common features underlying this diversity are that (a) these are complex systems, wherein the components (e.g., species, genes) have (developed) time-varying functional dependencies among each other (e.g., sharing resources and by-products, regulating biochemistry) that can be expressed as temporal networks, and (b) the effect of a perturbation, albeit initially localized in space and time, will potentially spread or cascade through the entire system. Predicting the spreading vulnerability of perturbations directly from topological complexity would be an asset—especially considering that the availability of real-world data on large perturbations are typically limited—for example, for mapping their tipping points [30], or alternatively, for tracing the boundaries of their safe operating spaces [31] that separate successful recovery from irreversible degradation.

Finally, we note that all the processes we considered in the paper for spreading dynamics are so-called point processes, meaning that they are processes that do not contain internal (memory-type) timescales. In the real world, however, dynamical processes running on top of the (temporal) networks will undoubtedly possess a diverse range of timescales (e.g., incubation period or time to become infectious for individual agents in case of pathogen spreading), and the process timescales will interact with the timescales of the changes in the network topology. We expect that the topological complexity of the networks to still be a crucial factor in dictating the spreading dynamics: the general nature of our methodological approach sets the stage for these applications in such wide and far-reaching areas, some of which are in the process of currently being investigated.

## ACKNOWLEDGMENTS

The authors thank Denny Borsboom, Michael X. Cohen, Sander van Doorn, Hans Heesterbeek, Mirjam Kretzschmar, and Paul van der Schoot for their useful remarks on the manuscript. The work has been financially supported by Dutch Research Council (NWO), and cosupported by Nederlandse Spoorwegen (NS) and ProRail, under Project No. 439.16.111.

All authors contributed to the research conceptualization. M.M.D., D.P., and R.S. conceived the mathematical principles. M.M.D. did the data analysis, with help of J.O. M.M.D. wrote the code for the data analyses and simulations, with help of R.S. M.M.D., and D.P. wrote first draft of the manuscript. All authors reviewed the final text.

## APPENDIX

The Appendix consist of four sections. Appendix A contains the formal derivation of the entropy of temporal entanglement. Appendix A contains the behavior of the entropy of temporal entanglement as a function of  $\Delta t$ . Appendix B contains information on the real-world temporal network data sets used in the paper. In Appendix C we elaborate on spreading processes playing out on top of temporal networks.

In particular, the data needed to perform the analyses in the paper are all open source and discussed in Appendix B.

### APPENDIX A: FORMAL DERIVATION OF THE ENTANGLEMENT ENTROPY

In this Appendix, we derive the building blocks  $Q^{(\text{in})}$  and  $Q^{(\text{out})}$  matrices for calculating the entanglement entropy. In Sec. 1, we do this for connected components of the network. In Sec. 2, we follow this up with the derivation of  $Q^{(\text{in})}$  and  $Q^{(\text{out})}$  matrices for the agents' precise contact networks at the snapshots as recorded in the data [e.g., as can be seen in Fig. 1(a) at  $t = 0$  in the main text], which we henceforth refer to as “fine structures” for brevity. We will witness that the  $Q$  matrices for both cases are determined from topological symmetry considerations, and are free of fitting parameters. The contribution of individual agents to entanglement is defined in Sec. 3.

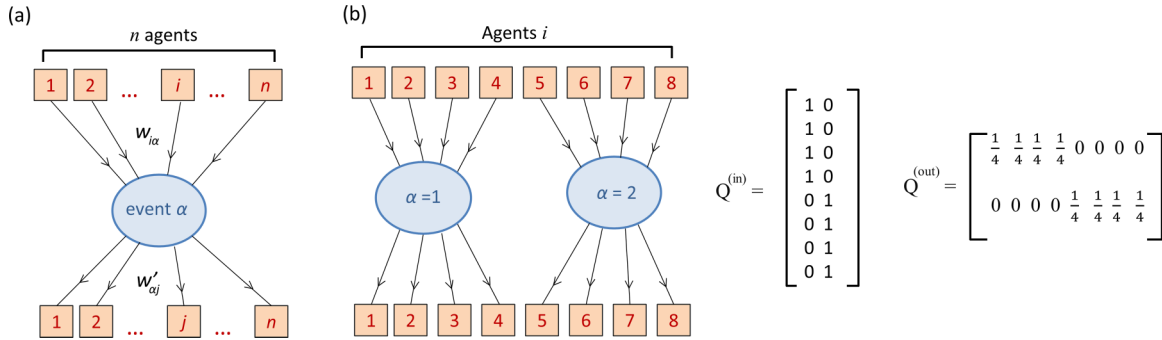


FIG. 5. (a) Event  $\alpha$  taking place at time  $t$  for one of the connected components with  $n$  agents, labeled by Roman indices. (b) As a working example, we consider the same event structure for eight agents at  $t = 0$  as in Fig. 1(b) in the main text of the paper.

**1. Entanglement entropy for connected components**

Let us start with a single connected component at time  $t$  [for example, as shown in Fig. 1(b) in the main text]. For this, it means that there is a single event  $\alpha$  containing  $n$  agents at time  $t$ . Following our convention regarding the agent strings as explained in the main text surrounding Fig. 1, such a situation is shown in Fig. 5(a). Therein, we denote the (topological) weight of a link from agent  $i$  coming into event  $\alpha$  by  $w_{i\alpha}$ , and similarly, the topological weight of a link exiting event  $\alpha$  and reaching agent  $j$  by  $w'_{\alpha j}$ . These weights are the elements of the  $Q^{(in)}$  and  $Q^{(out)}$  matrices, respectively. In this section, we determine these weights from the following considerations, and subsequently construct the corresponding  $Q$  and  $P$  matrices.

A1. The first observation is that the entanglement topology is invariant under time reversal. This implies

$$\frac{w_{1\alpha}}{w'_{\alpha 1}} = \frac{w_{2\alpha}}{w'_{\alpha 2}} = \dots = \frac{w_{n\alpha}}{w'_{\alpha n}} = c_\alpha, \tag{A1}$$

for some (yet unknown)  $c_\alpha$ .

A2. The second observation is that the entanglement topology is invariant under an exchange operation  $i \leftrightarrow j$  for all pairs of the agent identities  $i$  and  $j$ . This further implies  $w_{1\alpha} = w_{2\alpha} = \dots = w_{n\alpha} = w$ , for some (yet unknown)  $w$ .

A3. Finally,  $w$  and  $c$  are determined by considering random walker hops, as is standard in network science, in the following manner. (a) First,  $w_{i\alpha}$  is the probability for a random walker to start at agent  $i$  prior to time  $t$  and end at event  $\alpha$  at time  $t$  in one hop, meaning that  $w = 1$ . (b) Similarly,  $w_{\alpha j}$  is the probability of a random walker to start at event  $\alpha$  at time  $t$  and end at agent  $j$  subsequent to time  $t$ , yielding  $c_\alpha = n$ . Returning to the original notation from Fig. 5(a), this means that  $w_{i\alpha} = 1 \forall i$  and  $w'_{\alpha j} = 1/n \forall j$ .

Important to note here is that the random walkers only move forward in time; i.e., the link weights respect the direction of time.

Upon putting A1–A3 together, we can construct the relevant  $Q^{(in)}$ ,  $Q^{(out)}$ , and  $P$  matrices for this connected component. First,  $Q^{(in)}$ , whose  $i\alpha$ th element equals  $w_{i\alpha}$ , becomes an  $n \times 1$  matrix with all entries unity, and  $Q^{(out)}$ , whose  $\alpha j$ th element equals  $w'_{\alpha j}$ , becomes a  $1 \times n$  matrix with all elements equaling  $1/n$ . Next,  $P = Q^{(in)}Q^{(out)}$  becomes an  $n \times n$  matrix, for which all elements are equal to  $1/n$ , meaning that at time  $t$  all involved ( $= n$ ) agents contribute  $n \ln n$  to the entanglement entropy. [Note here that both  $Q^{(in)}$  and  $Q^{(out)}$

are row normalized, which makes  $P$  both row and column normalized. These normalizations stem from the conservation of random walkers—any random walker starting from any agent prior to time  $t$  must end up at some agent subsequent to time  $t$ .] In other words, the agents participating in the event are *maximally entangled* at time  $t$ : Indeed, if at time  $(t + 1)$  the same  $n$  agents also participate in an event together that involves no new agents, then ensured by the relation  $P^2 = P$ , the contribution of these  $n$  agents to entanglement entropy remains  $(n \ln n)/(N \ln N)$  also at time  $(t + 1)$ .

The method is trivially extended when there are multiple events taking place at time  $t$ , as shown for an example in Fig. 5(b) for eight agents, which, along with the corresponding  $P$  in Fig. 6, is then copied in Fig. 1(c) in the main text of the paper.

**2. Entanglement entropy for the fine structures**

Calculation of entanglement entropy involving the fine structures in the agents' contact networks at integer times can also be performed by constructing the corresponding  $Q^{(in)}$ ,  $Q^{(out)}$  and  $P = Q^{(in)}Q^{(out)}$  matrices—along very similar lines as in Appendix A. The procedure is in fact best illustrated by taking another working example, which we do in Fig. 7: Note that the fine structures correspond to those shown in Fig. 1(a)

$$P = \begin{bmatrix} \frac{1}{4} & \frac{1}{4} & \frac{1}{4} & \frac{1}{4} & 0 & 0 & 0 & 0 \\ \frac{1}{4} & \frac{1}{4} & \frac{1}{4} & \frac{1}{4} & 0 & 0 & 0 & 0 \\ \frac{1}{4} & \frac{1}{4} & \frac{1}{4} & \frac{1}{4} & 0 & 0 & 0 & 0 \\ \frac{1}{4} & \frac{1}{4} & \frac{1}{4} & \frac{1}{4} & 0 & 0 & 0 & 0 \\ 0 & 0 & 0 & 0 & \frac{1}{4} & \frac{1}{4} & \frac{1}{4} & \frac{1}{4} \\ 0 & 0 & 0 & 0 & \frac{1}{4} & \frac{1}{4} & \frac{1}{4} & \frac{1}{4} \\ 0 & 0 & 0 & 0 & \frac{1}{4} & \frac{1}{4} & \frac{1}{4} & \frac{1}{4} \\ 0 & 0 & 0 & 0 & \frac{1}{4} & \frac{1}{4} & \frac{1}{4} & \frac{1}{4} \end{bmatrix}$$

FIG. 6. The  $8 \times 8$   $P$  matrix constructed as  $P = Q^{(in)}Q^{(out)}$  from Fig. 5(b).

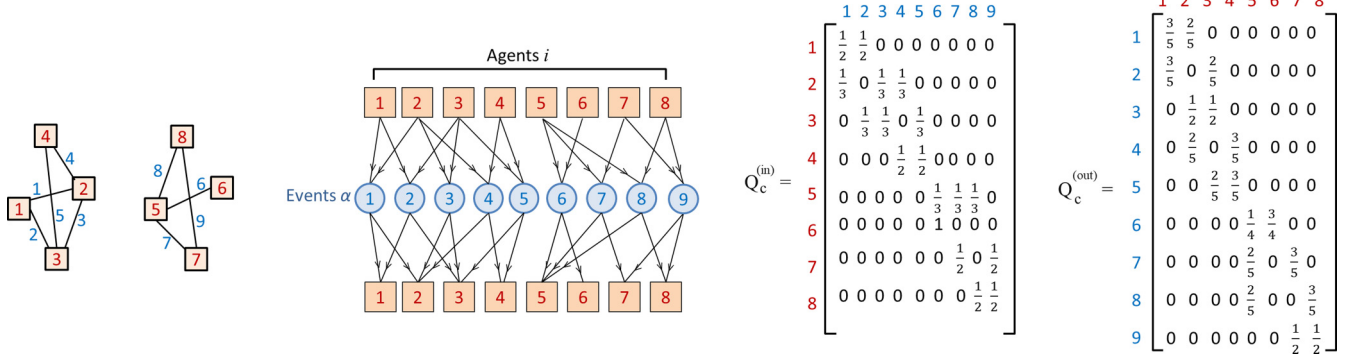


FIG. 7. Constructing the  $Q_c^{(\text{in})}$  and the  $Q_c^{(\text{out})}$  for the working example, containing the agents' actual contact network at  $t = 0$  in Fig. 1(a) of the main text.

at  $t = 0$  (in the main text of the paper). The key difference between the two working examples in Figs. 5 and 7 is that in the latter the fine structures of the agents' contact network at time  $t$  is possible to capture only by binary events (i.e., each event involves two agents, corresponding to the link between them). Nevertheless, we follow the same convention for the denoting the agents, the events, and the weights of the agent-to-event and event-to-agent links as we did in Appendix A.

First, the topology, as seen in Fig. 7, is again time-reversal invariant, which allows us to write, analogous to Eq. (A1),

$$\frac{w_{i\alpha}}{w'_{\alpha i}} = \frac{w_{j\alpha}}{w'_{\alpha j}} = c_\alpha, \quad (\text{A2})$$

where  $i$  and  $j$  are the two agents participating in (binary) event  $\alpha$ , for some (yet unknown)  $c_\alpha$ . [That said, the topology is no longer invariant under an exchange operation with regard to the agent identities  $i \leftrightarrow j$  as was the case in Fig. 5(a)]. Next, we assign  $w_{i\alpha}$  to be the probability for a random walker to start at agent  $i$  prior to time  $t$  and end at event  $\alpha$  at time  $t$ . Using the principle that, starting at agent  $i$ , the random walker chooses any of the connecting events with equal probability, we obtain  $Q_c^{(\text{in})}$ , whose  $i\alpha$ th element equals  $w_{i\alpha}$  (Fig. 7). Finally,  $Q_c^{(\text{out})}$ , whose  $\alpha j$ th element equals  $w'_{\alpha j}$ , and obeys Eq. (A2), is obtained by transposing  $Q_c^{(\text{in})}$  and subsequently row-normalizing it. The matrix  $Q_c^{(\text{out})}$ , obtained by means of this procedure, is also shown in Fig. 7.

The corresponding  $P$  matrix, obtained as  $P^{(\text{c})} = Q_c^{(\text{in})} Q_c^{(\text{out})}$  is shown in Fig. 8. It can be shown, using the above procedure to determine  $Q_c^{(\text{in})}$  and  $Q_c^{(\text{out})}$ , that

$$P_{ij}^{(\text{c})} = \frac{1}{\mathcal{K}_i + \mathcal{K}_j} \text{ for } i \neq j \text{ and } P_{ii}^{(\text{c})} = 1 - \sum_{j \neq i} P_{ij}^{(\text{c})}, \quad (\text{A3})$$

where  $\mathcal{K}_i$  is the degree of agent  $i$  in the contact network at time  $t$ . Clearly,  $P_{ij}^{(\text{c})} = 0$  if agents  $i$  and  $j$  are not in contact at time  $t$ . Note here that  $P^{(\text{c})}$ , just as in  $P$ , is row as well as column normalized (here too, the normalizations stem from conservation of random walkers—any random walker starting from any agent prior to time  $t$  must end up at some agent subsequent to time  $t$ ). Once  $P^{(\text{c})}$  is calculated in this way, the corresponding entanglement entropy  $S_c$  can be calculated following Eq. (2) in the main text.

A discussion on the differences between the  $P$  (Fig. 6) and the  $P^{(\text{c})}$  (Fig. 8) matrices is in order. The difference between the two stems from the fact that the agents within the two events in Fig. 5(b) are maximally entangled, which is not the case for the agents in Fig. 7. Mathematically, the difference lies in the fact that  $P^2 = P$  in contrast to  $[P^{(\text{c})}]^2 \neq P^{(\text{c})}$ .

In a more precise formulation, we note that while constructing  $P^{(\text{c})}$  by means of combining the probabilities of random walkers to start at agent  $i$  prior to time  $t$  and end at event  $\alpha$  at time  $t$ , or start at event  $\alpha$  at time  $t$  and end at agent  $i$  subsequent to time  $t$ , we have allowed the random walker to take one combined agent-to-agent hop across time  $t$ . From this, one would expect that if a large number of such sequential agent-to-agent random walker hops would be allowed while the agents' contact network remains the same over time [i.e., the same agent contact network holds at times  $t, (t+1), \dots, (t+k)$  for large  $k$ ] then the random walker starting prior to time  $t$  at agent  $i$  to reach all agents within the corresponding connected component subsequent to time  $(t+k)$  with equal probability. In fact, this is indeed the case, since

$$\lim_{k \rightarrow \infty} [P^{(\text{c})}]^k = P. \quad (\text{A4})$$

$$P^{(\text{c})} = \begin{bmatrix} \frac{3}{5} & \frac{1}{5} & \frac{1}{5} & 0 & 0 & 0 & 0 & 0 \\ \frac{1}{5} & \frac{13}{30} & \frac{1}{6} & \frac{1}{5} & 0 & 0 & 0 & 0 \\ \frac{1}{5} & \frac{1}{6} & \frac{13}{30} & \frac{1}{5} & 0 & 0 & 0 & 0 \\ 0 & \frac{1}{5} & \frac{1}{5} & \frac{3}{5} & 0 & 0 & 0 & 0 \\ 0 & 0 & 0 & 0 & \frac{7}{20} & \frac{1}{4} & \frac{1}{5} & \frac{1}{5} \\ 0 & 0 & 0 & 0 & \frac{1}{4} & \frac{3}{4} & 0 & 0 \\ 0 & 0 & 0 & 0 & \frac{1}{5} & 0 & \frac{11}{20} & \frac{1}{4} \\ 0 & 0 & 0 & 0 & \frac{1}{5} & 0 & \frac{1}{4} & \frac{11}{20} \end{bmatrix}$$

FIG. 8. The  $8 \times 8$   $P^{(\text{c})}$  matrix constructed as  $P^{(\text{c})} = Q_c^{(\text{in})} Q_c^{(\text{out})}$  from Fig. 7.

This limiting case is made possible by the condition that  $P^{(c)}$  matrices are row as well as column normalized (which in essence is the detailed balance condition in statistical physics, effected by the conservation of random walkers as stated above [32]).

Further reflection reveals that the subtleties regarding the differences between  $P$  and  $P^{(c)}$  arise due to the discreteness of the time snapshots. In the main text of the paper, we noted that real-world temporal network data are often sampled at some fixed interval  $\tau_s$ , and also that the random walker hops are coupled to  $\tau_s$ . Given that, in theory,  $\tau_s$  can be taken to be infinitesimally small (in comparison to the timescales of change in the topology of the agents' contact network), and that in real world, every interaction lasts for a finite amount of time, the limit (A4) ensures that  $P$  is the correct descriptor for measuring entanglement.

### 3. Contribution of a specific agent to entanglement

The contribution  $S_i$  of agent  $i$  to the entanglement entropy is the difference between the entanglement entropy when string  $i$  is embedded in the temporal network and that when string  $i$  is removed from of the temporal network. Note that two entanglements of agent  $i$  at two different snapshots, with agents  $j$  and  $k$  respectively, makes agent  $i$  an in-between temporal stop for agents  $j$  and  $k$ . With this in mind,  $S_i$  can be seen as *a measure of betweenness of agent  $i$  in a temporal network*.

The quantity  $S_i$  can be calculated as follows. For every time snapshot, we construct the  $P$  matrices and the corresponding  $P^{(-i)}$  matrices by replacing all the  $i$ th row and column elements of the  $P$  matrices by zeros, except the diagonal element  $P_{ii}$ . We then row normalize both of them separately to obtain the  $P$  and the  $P^{(-i)}$  matrices, and construct the product matrices  $\wp(t, \Delta t) \equiv P(t)P(t+1) \dots P(t+\Delta t)$  and  $\wp^{(-i)}(t, t+\Delta t) \equiv P^{(-i)}(t)P^{(-i)}(t+1) \dots P^{(-i)}(t+\Delta t)$ . This is followed by correspondingly calculating  $S(t, \Delta t)$  and  $S^{(-i)}(t, \Delta t)$  using Eq. (2). This yields us

$$S_i(t, \Delta t) = S(t, \Delta t) - S^{(-i)}(t, \Delta t). \quad (\text{A5})$$

### APPENDIX B: ENTANGLEMENT ENTROPY AS A FUNCTION OF $\Delta t$

In the main text, especially in Fig. 3, we have analyzed the evolution of entanglement entropy. In this section, we investigate the highest rate at which entropy can increase with the time interval size  $\Delta t$ , which we in the end extrapolate to

the special case of a perfect tree—i.e., a system we argue has the maximum possible entropy growth with time.

Although in real-world networks, event sizes vary considerably, for the sake of an illustration, given a certain initialization time  $t$ , let us consider the case where the event sizes are constant ( $= n$ ) for  $\Delta t = 1$ . Following Fig. 1, all rows of  $\wp$  will have exactly  $n$  entries containing  $\frac{1}{n}$ , and 0 elsewhere, leading to

$$S_{\text{tree}}(t, \Delta t = 1) = -\frac{1}{N \ln N} N n \left( \frac{1}{n} \ln \frac{1}{n} \right) = \frac{\ln n}{\ln N}.$$

Extending this to higher values of  $\Delta t$  requires more formality. To this end, we consider an event  $\mathcal{E}$  of size  $n_{\mathcal{E}}$  at some time  $t' = t + \Delta t$  where  $\Delta t > 1$ , and conceptually imagine that agents from different groups, labeled by colors such as red, blue, etc., participate. We define a group  $\mathcal{G}$  as follows: In between times  $t$  and  $t'$ ,  $\forall i$  belonging to one group, and  $\forall j$  belonging to another, there is no event where both  $i$  and  $j$  are temporally connected. Prior to time  $t'$ , let us denote the number of red agents (i.e., belonging to the red group  $\mathcal{G}_R$ ) by  $\mathcal{N}_R$ , the number of blue agents (i.e., belonging to the blue group  $\mathcal{G}_B$ ) by  $\mathcal{N}_B$ , and so on. Similarly, the number of red agents participating in event  $\mathcal{E}$  at time  $t'$  is given by  $n_R$  (forming the corresponding subgroup  $g_R$ ), the number of blue agents participating in event  $\mathcal{E}$  at time  $t'$  is given by  $n_B$  (forming the corresponding subgroup  $g_B$ ), and so on. Clearly,

$$n_R + n_B + \dots = n. \quad (\text{B1})$$

We also label the elements of  $\wp(t, \Delta t - 1)$  belonging to a given colored group by indices of the same color; e.g., we reindex the red agents by red indices  $1_R, 2_R, \dots, \mathcal{N}_R$ , of which the agents  $1_R, 2_R, \dots, n_R$  participate in the event. Then the elements of the  $\wp(t, \Delta t - 1)$  matrix corresponding to the red group of agents can be extracted to form an  $\mathcal{N}_R \times \mathcal{N}_R$  matrix. Let us denote these elements by the notation  $p_{ij}$ , with  $1_R \leq (i, j) \leq \mathcal{N}_R$ . Then the following relations will hold:

$$\sum_{i=1_R}^{\mathcal{N}_R} p_{ij}(t-1) = 1, \quad i \in \mathcal{G}_R, j \in g_R;$$

$$\sum_{i=1_B}^{\mathcal{N}_B} p_{ij}(t-1) = \dots = 1, \quad i \in \mathcal{G}_B, j \in g_B; \dots$$

These relations simply follow from the fact that  $\wp(t, \Delta t - 1)$  is column normalized, having noted that  $\wp_{ij}(t, \Delta t - 1) = 0$  when agents  $i$  and  $j$  belong to two different (ly colored) groups.

Subsequent to the event at time  $t$ , for an agent  $j \in \mathcal{E}$  the elements of  $P(t)$  will be given by

$$p_{ij}(t) = \frac{1}{n_{\mathcal{E}}} \begin{cases} \sum_{j'=1_R}^{n_R} p_{ij'}(t-1) & i \in \mathcal{G}_R, j' \in g_R \\ \sum_{j'=1_B}^{n_B} p_{ij'}(t-1) & i \in \mathcal{G}_B, j' \in g_B \\ \dots & \dots \end{cases}, \quad (\text{B2})$$

and is independent of  $j$  [i.e.,  $p_{ij}(t) \equiv p_i(t)$ ]. This allows us to express the corresponding change in entropy due to the event  $\mathcal{E}$ , by separating the agents in different (ly colored) subgroups, as

$$\Delta S = \frac{1}{N \ln N} \left\{ \left[ n_{\mathcal{E}} \sum_{i=1_R}^{\mathcal{N}_R} p_i(t) \ln p_i(t) - \sum_{i=1_R}^{\mathcal{N}_R} \sum_{j=1_R}^{n_R} p_{ij}(t-1) \ln p_{ij}(t-1) \right] + \left[ n_{\mathcal{E}} \sum_{i=1_B}^{\mathcal{N}_B} p_i(t) \ln p_i(t) - \sum_{i=1_B}^{\mathcal{N}_B} \sum_{j=1_B}^{n_B} p_{ij}(t-1) \ln p_{ij}(t-1) \right] + \dots \right\}. \quad (\text{B3})$$

Using Eq. (B2) to replace  $p_{ij}(t)$  in Eq. (B3), and thereafter having dropped the  $(t-1)$  argument for the matrix elements, we have

$$\Delta S = \frac{n_{\mathcal{E}} \ln n_{\mathcal{E}}}{N \ln N} + \frac{1}{N \ln N} \left\{ \underbrace{\left[ \sum_{i=1_R}^{\mathcal{N}_R} \sum_{j=1_R}^{n_R} p_{ij} \ln p_{ij} - \sum_{i=1_R}^{\mathcal{N}_R} \left( \sum_{j=1_R}^{n_R} p_{ij} \right) \ln \left( \sum_{j=1_R}^{n_R} p_{ij} \right) \right]}_{C_R} + \underbrace{\left[ \sum_{i=1_B}^{\mathcal{N}_B} \sum_{j=1_B}^{n_B} p_{ij} \ln p_{ij} - \sum_{i=1_B}^{\mathcal{N}_B} \left( \sum_{j=1_B}^{n_B} p_{ij} \right) \ln \left( \sum_{j=1_B}^{n_B} p_{ij} \right) \right]}_{C_B} + \dots \right\}. \quad (\text{B4})$$

Given that  $p_{ij} \leq 1$ , it is easily argued from Eq. (B4) that  $C_R, C_B$ , etc., terms are  $\leq 0$ : The only case when they can be zero is when  $n_R, n_B$ , etc., either 0 or 1. This in turn means that an event can maximally contribute to the entanglement entropy only when, for every agent pair  $(i, j)$  participating in the event, between  $t$  and  $t'$  there exists no event that both  $i$  and  $j$  are temporally connected to.

Note, however, that this condition is not possible to maintain for an arbitrary temporal depth of between  $t$  and  $t + \Delta t$ . A toy case where this is possible—returning to the one we started this section with—is with fixed event size  $n$  and also fixed event frequency  $n$  per snapshot, requiring the condition  $N = n^k$  to be satisfied for some integer  $k$ . We illustrate the procedure with an example below. When increasing  $\Delta t$  to 2 in that toy example, we add an extra time step. For the system that is a perfect tree in the temporal domain, any agents that have participated in events at  $\Delta t = 1$ , do not participate in an event at  $\Delta t = 2$ ; instead, all  $n$  agents from any event in the first time step participate in  $n$  separate events. This ensures that the all rows of the  $\wp$  matrix have exactly  $n^2$  elements with entries  $\frac{1}{n^2}$ , resulting in  $S(t, \Delta t = 2) = 2 \frac{\ln n}{\ln N}$ . Continuing this for any value of  $\Delta t$ , this can be generalized to

$$S_{\text{tree}}(t, \Delta t) = -\frac{1}{N \ln N} N n^{\Delta t} \left( \frac{1}{n^{\Delta t}} \ln \frac{1}{n^{\Delta t}} \right) = \Delta t \frac{\ln n}{\ln N},$$

leading to a linear relationship between  $S$  and  $\Delta t$  for a perfect tree in the temporal domain.

From a point of view of analyzing spreading dynamics, the perfect tree is the system with the highest spreading vulnerability. For a perfect tree in the temporal domain, agents only meet agents that do not have a (higher order) connection in common in the past. For the application of rumor spreading, for example, in a perfect tree, people that *know* the rumor

will therefore only meet people that *do not know* the rumor—obtaining the fastest possible spread of the rumor.

### APPENDIX C: REAL-WORLD TEMPORAL NETWORK DATASETS USED IN THE PAPER

In Fig. 1 of the main text, we use a network constructed by hand for illustration purposes. In Figs. 2 and 3 of the main text, we use temporal network data from real-world systems. In this section, we discuss the preprocessing and availability of these data sets.

#### 1. High school and primary school

In Fig. 2 of the main text, we use data on the interactions among students of a high school and a primary school. Both data sets are frequently used in network science papers. The high school data are referred to as the “Thiers13” data set [26], from which we use two days in the analysis, and the primary school data are the “LyonSchool” data set [2,33], from which we also use two days of data in the table in Fig. 3(b) of the main text. Both are freely accessible at the Sociopatterns project website [34]. Agent interactions in these data sets are defined as close face-to-face proximity of students and teachers using wearable sensors and proximity-sensing infrastructure based on radio frequency identification devices. In the table in Fig. 3(b) of the main text, we also use a second high school data set (also from the Sociopatterns project) from 2011, referred to as “Thiers11,” from which we use four days in the analysis. The sampling time interval  $\tau_s$  for these data sets is 20 s.

## 2. Other Sociopatterns data sets

Data from the scientific conference, hospital, and workplaces (2013) and (2015) are also accessible via the Sociopatterns project and are often referred to as the SFHH conference, LH10, InVs13, and InVs15 data sets. The scientific conference refers to the 2009 SFHH conference in Nice, France (June 4–5, 2009) [1,5]. The workplace data sets InVs13 and InVs15 were experiments conducted in French office buildings in 2013 and 2015 respectively [25]. The hospital data set contains the temporal network of contacts among patients and health-care workers (HCWs) and among HCWs in a hospital ward in Lyon, France, from Monday, December 6, 2010, at 1:00 pm to Friday, December 10, 2010, at 2:00 pm—we use four separated days in our analysis from this time interval. The study included 46 HCWs and 29 patients [28]. The sampling time interval  $\tau_s$  for these data sets is 20 s.

## 3. High-energy physics citations

The citations network we analyze in the paper is from the e-print arXiv server HEP-PH (high energy physics phenomenology) and covers all the citations within a data set of 34 546 papers with 421 578 edges [35]. Because of the enormous amount of agents (i.e., papers) and (temporal) links, we only use a subset of this data set. The data set comprises papers over approximately 10 years of data. We only use papers between 11 March 1996 and 3 Aug 1998. These dates are obtained by taking 10 000 interactions in approximately the middle of the time series (to best relate to the temporal dynamics of this system). This results in a much smaller number of 4 052 papers (approximately 10% of the total). If a paper  $i$  cites paper  $j$ , we treat this as an interaction between these two papers. The sampling time interval  $\tau_s$  for these data sets is in days.

## 4. Baboons

The baboons temporal network we analyzed is from an experiment on a group of 20 Guinea baboons living in an enclosure of a primate center in France, between June 13th 2019 and July 10th 2019 [27]. Only 13 out of the 20 baboons wore proximity sensors, which are the data we use for this analysis. In our analysis, we use the first five days of this data set. The sampling time interval  $\tau_s$  for these data sets is 20 s.

## 5. Sparrows

The sparrows data set is from a study at the University of California, Santa Cruz Arboretum [36]. The sparrows arrive there in October–November and depart for their breeding grounds in March–April each year. The study spanned three nonbreeding seasons: January–March 2010 (season 1), October 2010–February 2011 (season 2), and October 2011–April 2012 (season 3). Each season, the authors captured birds using baited traps and attached individually unique combinations of color bands. In season 2, they did not band any birds between October and December 2010. Network edges are found based on comemberships between flocks (defined as a group of individuals found within a single 5-m radius) by identifying

the color-banded individuals in each flock. Data are available at  $\tau_s = 1$  day.

## 6. Irvine social app

This data set is composed of private messages sent on an online social network at the University of California, Irvine. Users could search the network for others and then initiate conversation based on profile information. An edge  $(i, j, t)$  means that user  $i$  sent a private message to user  $j$  at time  $t$  [37]. The data as a whole span approximately 195 days. As with the aforementioned Citations data set, for this analysis, we focused on only part of the data set to improve computational speed. In particular, we used the first 34 days, resulting in a set of 25 000 interactions and 1136 unique agents (users). The time is aggregated to  $\tau_s = 6$  h.

## 7. Art fair

The art fair data were gathered during “Smart Distance Lab: The Art Fair” between August 28 and 30, 2020, in Amsterdam, the Netherlands [38]. The data set consists of eight experiments, where various conditions such as walking direction, face masks, and proximity alerting systems were varied. We use the data from the wearable sensors that defined an interaction by two people coming in the proximity of less than 1.5 m. The data set is available on Figshare and in a MySQL database. The sampling time interval  $\tau_s$  for this data set is 1 s.

## APPENDIX D: SPREADING PROCESSES ON TOP OF TEMPORAL NETWORKS

In order to reveal the relationship between the entanglement entropy and the dynamical processes playing out on top of the network, we simulate three models describing three different (stochastic) processes on the real-world systems in Fig. 3 and Table 1 of the main text. The results of the simulations, reported in the main text, have been obtained by performing ensembles of 25 re-initialized model runs (per initialization time  $t$ ) over 80% of the full time window per system as starting points  $t$ , using  $\Delta t = 12$  time steps for the correlations in Fig. 3(b) in the main text, and 60 time steps for the visualizations in Figs. 3(c) and 3(d). Only ensemble averages are reported in the main text. For most data sets, this procedure is repeated over multiple subsets. For example, the high school data Thiers13 contains 5 days of data. Those days are individually run using this ensemble procedure, and the average across those days is shown in the table in Fig. 3(b) of the main text. Below, we describe the stochastic models. For all models, the number of agents is denoted by  $N$ .

### 1. Majority vote

For the first model, we simulate the propagation of opinions on a dilemma, which is associated with spreading of information, such as (fake) news, memes, or political opinions. The opinion of agent  $i$  at time  $t$  can have values 0 or 1. We denote the overall fraction of agents having opinion 0 with  $f_0$ , and analogously we define  $f_1$ . At initialization (starting time  $t$ , interval size  $\Delta t = 0$ ), we start with half of

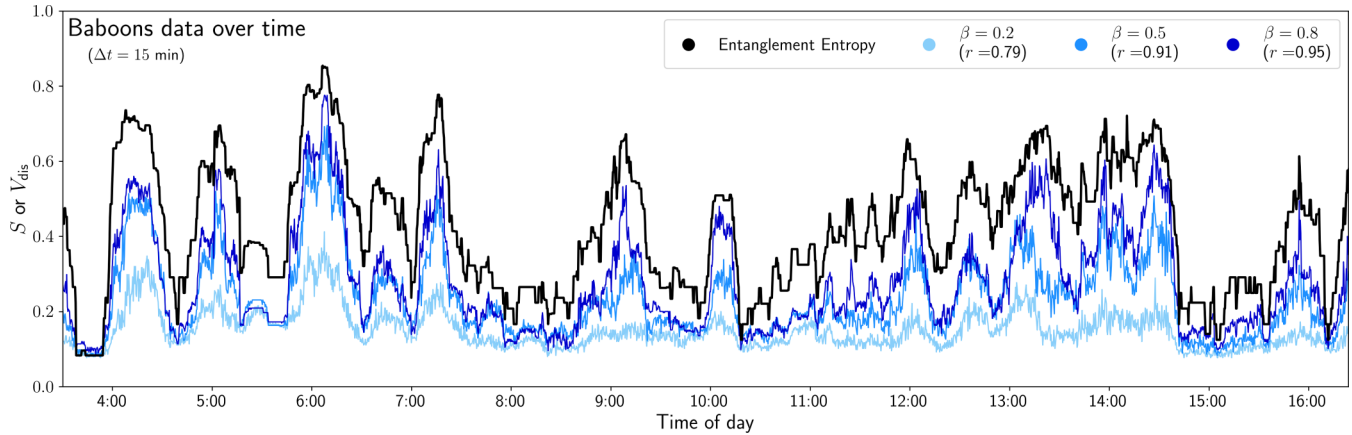


FIG. 9. Evolution of entanglement entropy  $S$ , and the state variable  $V_{\text{dis}}$ , for three values of  $\beta$ , using  $\Delta t = 15$  min, for day 2 in the Baboons data set. Pearson's correlation values ( $r$ ) are also noted in the figure (which are the values only for this particular day). Note that Fig. 3(b) of the main text uses 5 days of the Baboons data set, leading to a slightly smaller Pearson's correlation value for  $\beta = 0.8$ , namely 0.93.

the population having opinion 0, and the other half opinion 1. The agent interactions are specified as they are defined by the (real-world) temporal network's topology. At each event, all agents change their opinion to the opinion of the majority of the participants. For example, if in an event with three agents the opinions are 001, then the third agent will change its opinion to 0. If the opinions are tied, all participants will swap to a single opinion, chosen at random. If there is only one single agent in an event, its opinion will remain the same. No noise is introduced. We define a single state variable that is dependent on the starting time of the model ( $t$ ) and the time interval ( $\Delta t$ ) that is used to progress it from  $t$  onward:

$$V_{\text{maj}}(t, \Delta t) = 2[\max(f_0(t, \Delta t), f_1(t, \Delta t)) - 0.5].$$

The subtraction of 0.5 and subsequent multiplication with 2 make sure that  $V_{\text{maj}} \in [0, 1]$ , which is a standardized form for easy comparison to the entanglement entropy.

## 2. Transport delay

The second model concerns the propagation of a continuous variable through interactions (events), all event participants will attain the highest value among them. This relates to various real-world phenomena, such as transportation delays (hence the title of this model), in which transport assets (such as a physical train and a driver to drive it; assets may need to come from different physical locations [39] and have to wait for the maximally delayed one—assigning all assets in an event with a newly generated delay that equals the highest of all the delays in that event. (Another example is the spread of dominant genes in phylogenetics.) At the start of the model, all agents are given a random number between 0 and 1, which we refer to as the delay  $d_i$  of agent  $i$ , which propagates as per the above rule. Over time, the average delay will increase

up to the maximum existing delay. We define a state variable, again dependent on  $t$  and  $\Delta t$ :

$$V_{\text{del}}(t, \Delta t) = 2 \left[ \frac{1}{N} \sum_{i=1}^N d_{i=1}(t, \Delta t) - 0.5 \right],$$

which has the same standardization as the state variable of the majority-vote system, to bring  $V_{\text{del}}$  between 0 and 1.

## 3. Infectious disease

While numerous infectious disease models for networks exist, we chose the simple susceptible-infected (SI) model. Each of the model's agents  $i$  can be in either one of two states  $q_i$ : susceptible ( $q_i = 0$ ) or infected ( $q_i = 1$ ). There is no exposed or recovered state, as commonly used in epidemiology. Each model run is initialized with 10% (randomly chosen) agents being infected. Upon interaction in an event, if one of the participants is infected, there is a probability  $\beta$  of other (susceptible) participants becoming infected as well. We define a state variable dependent on  $t$  and  $\Delta t$ , which is the average status  $q$  over all agents:

$$V_{\text{dis}}(t, \Delta t) = \frac{1}{N} \sum_{i=1}^N q_i(t, \Delta t),$$

which is a number between 0 (no infected) and 1 (all agents infected).

Clearly  $\beta$  is a parameter for the spreading of the pathogen. For the main text of the paper, we have chosen  $\beta = 0.8$ . For the Baboons data set, below we present the data for two additional values of  $\beta$  in Fig. 9. While the Pearson's correlation between  $S$  and  $V_{\text{dis}}$  decreases with decreasing  $\beta$ , the correlation still remains substantial even for  $\beta$  as low as 0.2.

- [1] C. Cattuto, W. Van den Broeck, A. Barrat, V. Colizza, J.-F. Pinton, and A. Vespignani, Dynamics of person-to-person interactions from distributed RFID sensor networks, *PLOS ONE* **5**, e11596 (2010).
- [2] J. Stehlé, N. Voirin, A. Barrat, C. Cattuto, L. Isella, J. Pinton, M. Quaggiotto, W. Van den Broeck, C. Régis, B. Lina, and P.

Vanhems, High-resolution measurements of face-to-face contact patterns in a primary school, *PLOS ONE* **6**, e23176 (2011).

- [3] E. Almaas, B. Kovács, T. Vicsek, Z. N. Oltvai, and A. L. Barabási, Global organization of metabolic fluxes in the bacterium *Escherichia coli*, *Nature (London)* **427**, 839 (2004).

- [4] N. Yosef and A. Regev, Impulse control: Temporal dynamics in gene transcription, *Cell* **144**, 886 (2011).
- [5] J. Stehlé, N. Voirin, A. Barrat, C. Cattuto, V. Colizza, L. Isella, C. Régis, J.-F. Pinton, N. Khanafer, W. Van den Broeck, and P. Vanhems, Simulation of an SEIR infectious disease model on the dynamic contact network of conference attendees, *BMC Medicine* **9**, 87 (2011).
- [6] J. A. Firth, J. Hellewell, P. Klepac, S. Kissler, M. Jit, K. E. Atkins, S. Clifford, C. J. Villabona-Arenas, S. R. Meakin, C. Diamond, N. I. Bosse, J. D. Munday, K. Prem, A. M. Foss, E. S. Nightingale, K. v. Zandvoort, N. G. Davies, H. P. Gibbs, G. Medley, A. Gimma *et al.*, Using a real-world network to model localized COVID-19 control strategies, *Nat. Med.* **26**, 1616 (2020).
- [7] W. Wang, Y. Ma, T. Wu, Y. Dai, X. Chen, and L. A. Braunstein, Containing misinformation spreading in temporal social networks, *Chaos* **29**, 123131 (2019).
- [8] T. Klausberger and P. Somogyi, Neuronal diversity and temporal dynamics: The unity of hippocampal circuit operations, *Science* **321**, 53 (2008).
- [9] S. Rakshit, B. K. Bera, and D. Ghosh, Synchronization in a temporal multiplex neuronal hypernetwork, *Phys. Rev. E* **98**, 032305 (2018).
- [10] A. Badie-Modiri, M. Karsai, and M. Kivela, Efficient limited-time reachability estimation in temporal networks, *Phys. Rev. E* **101**, 052303 (2020).
- [11] M. Mancastropa, A. Vezzani, M. A. Muñoz, and R. Burioni, Burstiness in activity-driven networks and the epidemic threshold, *J. Stat. Mech.: Theory Exp.* (2019) 053502.
- [12] N. Masuda and P. Holme, Small inter-event times govern epidemic spreading on networks, *Phys. Rev. Research* **2**, 023163 (2020).
- [13] A. Li, L. Zhou, Q. Su, S. P. Cornelius, Y.-Y. Liu, L. Wang, and S. A. Levin, Evolution of cooperation on temporal networks, *Nat. Commun.* **11**, 2259 (2020).
- [14] P. Holme and J. Saramäki, Temporal networks, *Phys. Rep.* **519**, 97 (2012).
- [15] C. S. Riolo, J. S. Koopman, and S. E. Chick, Methods and measures for the description of epidemiologic contact networks, *J. Urban Health* **78**, 446 (2001).
- [16] L. Isella, J. S. A. Barrat, C. Cattuto, J.-F. Pinton, and W. Van den Broeck, What's in a crowd? Analysis of face-to-face behavioral networks, *J. Theor. Biol.* **271**, 166 (2011).
- [17] N. Perra, B. Gonçalves, R. Pastor-Satorras, and A. Vespignani, Activity driven modeling of time varying networks, *Sci. Rep.* **2**, 469 (2012).
- [18] A. Li, S. P. Cornelius, Y.-Y. Liu, L. Wang, and A.-L. Barabási, The fundamental advantages of temporal networks, *Science* **358**, 1042 (2017).
- [19] M. Girvan and M. E. J. Newman, Community structure in social and biological networks, *Proc. Natl. Acad. Sci. USA* **99**, 7821 (2002).
- [20] N. Masuda and P. Holme, Predicting and controlling infectious disease epidemics using temporal networks, *F1000Prime Rep.* **5**, 6 (2013).
- [21] M. Rosvall and C. T. Bergstrom, Mapping change in large networks, *PLOS ONE* **5**, e8694 (2010).
- [22] T. P. Peixoto and M. Rosvall, Modelling sequences and temporal networks with dynamic community structures, *Nat. Commun.* **8**, 582 (2017).
- [23] H. Kim and R. Anderson, Temporal node centrality in complex networks, *Phys. Rev. E* **85**, 026107 (2012).
- [24] P. J. Mucha, T. Richardson, K. Macon, M. A. Porter, and J.-P. Onnela, Community structure in time-dependent, multiscale, and multiplex networks, *Science* **328**, 876 (2010).
- [25] M. Génois and A. Barrat, Can co-location be used as a proxy for face-to-face contacts? *EPJ Data Sci.* **7**, 11 (2018).
- [26] R. Mastrandrea, J. Fournet, and A. Barrat, Contact patterns in a high school: A comparison between data collected using wearable sensors, contact diaries, and friendship surveys, *PLOS ONE* **10**, e0136497 (2015).
- [27] V. Gelardi, J. Godard, D. Paleressompouille, N. Claidiere, and A. Barrat, Measuring social networks in primates: Wearable sensors versus direct observations, *Proc. R. Soc. A* **476**, 20190737 (2020).
- [28] P. Vanhems, A. Barrat, C. Cattuto, J. Pinton, N. Khanafer, C. Régis, B.-A. Kim, B. Comte, and N. Voirin, Estimating potential infection transmission routes in hospital wards using wearable proximity sensors, *PLoS ONE* **8**, e73970 (2013).
- [29] M. M. Dekker, T. F. Blanken, F. Dablander, J. Ou, D. Borsboom, and D. Panja, Quantifying agent impacts on contact sequences in social interactions, *Sci. Rep.* **12**, 3483 (2022).
- [30] V. Dakos, B. Matthews, A. P. Hendry, J. Levine, N. Loeuille, J. Norberg, P. Nosil, M. Scheffer, and L. De Meester, Ecosystem tipping points in an evolving world, *Nature Ecol. Evol.* **3**, 355 (2019).
- [31] J. Rockström, W. Steffen, K. Noone, Å. Persson, F. S. Chapin, E. F. Lambin, T. M. Lenton, M. Scheffer, C. Folke, H. J. Schellnhuber, B. Nykvist, C. A. de Wit, T. Hughes, S. van der Leeuw, H. Rodhe, S. Sörlin, P. K. Snyder, R. Costanza, U. Svedin, M. Falkenmark *et al.*, A safe operating space for humanity, *Nature (London)* **461**, 472 (2009).
- [32] N. van Kampen, *Stochastic Processes in Physics and Chemistry*, 3rd ed. (Elsevier, Amsterdam, 2007), pp. 193–218.
- [33] V. Gemmetto, A. Barrat, and C. Cattuto, Mitigation of infectious disease at school: Targeted class closure vs school closure, *BMC Infect. Dis.* **14**, 695 (2014).
- [34] <http://www.sociopatterns.org/datasets/>.
- [35] J. Gehrke, P. Ginsparg, and J. Kleinberg, Overview of the 2003 KDD cup, *SIGKDD Explor. Newsl.* **5**, 149 (2003).
- [36] D. Shizuka, A. S. Chaine, J. Anderson, O. Johnson, I. M. Laursen, and B. E. Lyon, Across-year social stability shapes network structure in wintering migrant sparrows, *Ecol. Lett.* **17**, 998 (2014).
- [37] P. Panzarasa, T. Opsahl, and K. M. Carley, Patterns and dynamics of users behavior and interaction: Network analysis of an online community, *J. Am. Soc. Inform. Sci. Technol.* **60**, 911 (2009).
- [38] C. C. Tanis, N. M. Leach, S. J. Geiger, F. H. Nauta, F. Dablander, F. van Harreveld, S. de Wit, G. Kanters, J. Knoppers, D. A. W. Markus, R. R. M. Bouten, Q. H. Oostvogel, M. J. Boersma, M. V. van der Steenhoven, D. Borsboom, and T. F. Blanken, Smart Distance Lab's art fair, experimental data on social distancing during the COVID-19 pandemic, *Sci. Data* **8**, 179 (2021).
- [39] M. M. Dekker and D. Panja, Cascading dominates large-scale disruptions in transport over complex networks, *PLOS ONE* **16**, e0246077 (2021).